Control of a Telescope Mount for Astronomical Observations and LEO Satellite Tracking

B. Espinoza-Garcia[1], P.R. Yanyachi[2], Jaime Gerson Cuba Mamani[3]
[1, 2, 3]*Instituto de Investigación Astronómico y Aeroespacial Pedro Paulet, Universidad Nacional* de San Agustín de Arequipa, Arequipa, Peru
bespinozag@unsa.edu.pe[1], raulpab@unsa.edu.pe[2], jcubam@unsa.edu.pe[3]

***Abstract*—This paper presents the development and simulation of a 2-DOF spherical telescope for astronomical observations and LEO satellite tracking, modeled using the Euler-Lagrange methodology. An adaptive PID controller, optimized with genetic algorithms, ensures robust control. The simulations demonstrate that the telescope's response converges asymptotically without control input chattering, effectively handling the dynamics of the system.**

***Index Terms*—Telescope, adaptive control, Astronomical observations**

I. Introduction

Astronomy and astrophysics in Peru are advancing under the supervision of the National Commission for Aerospace Research and Development (CONIDA) through its Directorate of Astrophysics (DIAST). This division focuses on areas such as Observational Astronomy, Space Weather, and Space Surveillance [1]. A facility contributing to this progress is the Moquegua Astronomical Observatory, home to the largest telescope in Peru, featuring a 1-meter diameter mirror. The observatory, located in Cambrune, Carumas, conducts systematic observations of celestial bodies using specialized cameras and spectrometers, enabling the identification of various elements and compounds in space.

On the other hand, Arequipa was home to the Carmen Alto Observatory (1890-1926), which made significant contributions to astronomy, including the discovery of 1,130 nebulae, Saturn's moon Phoebe, and the cataloging of the spectra of 250,000 stars [2]. Since 1957, the region has continued its astronomical legacy through an agreement between the Smithsonian Institution of Washington D.C. and the Universidad Nacional de San Agustín de Arequipa, which established a ground station for laser satellite tracking (LRS) to monitor Low Earth Orbit (LEO) satellites, making it one of the first such stations in the Southern Hemisphere.

In 2007, the Transportable Laser Ranging System (TLRS-3) was installed, further enhancing satellite tracking capabilities. Operating as part of the International Laser Ranging Service (ILRS) network, the TLRS-3 provides data used to calculate precise satellite orbits, monitor tectonic motion and deformation, and determine the Earth's gravity field and Earth Orientation Parameters (EOP) [3]. The system consists of a telescope mount that fires a green laser beam at satellites equipped with retro-reflectors, which reflect the beam to the station (Fig. 1). By measuring the light's travel time, the system determines the satellite's position. Given the high velocity of LEO satellites, the system requires an exceptionally precise pointing mechanism to ensure accurate tracking.

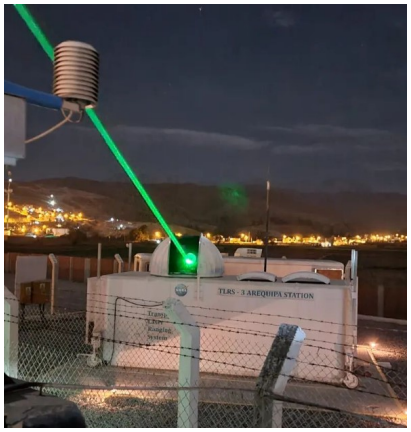

Fig. 1: The TLRS-3 system, located in Arequipa, Peru, operates under an agreement between NASA and the Universidad Nacional de San Agustin de Arequipa (UNSA).

Given the above, this paper proposes leveraging and replicating the TLRS-3 telescope mount by enhancing its control system, which manages azimuth and elevation movements to accurately point the telescope at various sky locations (Fig. 2). This controller design can also be applied to astronomical observations. To achieve this, the telescope is initially modeled using the Euler-Lagrange method (Section II). An azimuth and elevation control algorithm, incorporating an adaptive PID controller and a genetic algorithm (GA) for offline tuning, is presented in Section III. Numerical simulation results for the telescope with GA-tuned control are provided in Section IV. Finally, Section V summarizes the conclusions regarding the proposed control algorithm.

II. Mathematical Models

A spherical coordinates telescope can be modeled as a rotational robot with two degrees of freedom (DOF).

A. Kinematic Models

The kinematic model describes the position and orientation of the end effector without considering external forces [4], [5]. For the telescope under study, four reference frames have been defined, as depicted in Fig. 2. The initial frame, denoted as F_0, is defined using North, East, and Up (NEU) coordinates for the telescope's position, where the X_0 axis points North, Y_0 points East, and Z_0 points Up. Frames F_1 and F_2 share the same origin, while F_3 is located at the end of the telescope. The joint angles q_1 and q_2 represent the azimuth and elevation angles of the telescope, respectively. The Denavit-Hartenberg (DH) parameters for the proposed telescope are defined in Table I following the guidelines of [6].

TABLE I: Telescope DH parameters

Link Number	Parameters			
	θ	**d**	**a**	α
1	q_1	L_1	0	0
2	0	0	0	pi/2
3	q_2	0	L_2	0

The transformation matrix from frame F_0 to F_3 calculated using the D-H parameters is denoted as ${}^0A_3$, defined in (1).

$$ {}^0A_3 = \begin{bmatrix} c_1c_2 & -c_1s_2 & s_1 & L_2c_1c_2 \\ s_1c_2 & -s_1s_2 & -c_1 & L_2s_1c_2 \\ s_2 & c_2 & 0 & L_2s_2 + L_1 \\ 0 & 0 & 0 & 1 \end{bmatrix} \tag{1} $$

Here, $s_1 = \sin(q_1)$, $c_1 = \cos(q_1)$, $s_2 = \sin(q_2)$, $c_2 = \cos(q_2)$. Additionally, L_1 and L_2 are defined in Fig. I as link lengths.

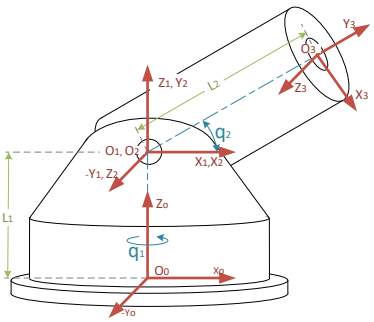

Fig. 2: Telescope Mount modeled as 2DOF robotic Arm.

B. Dynamical Models

The dynamical model, derived using the Euler-Lagrange method [7], provides information about the torques and forces necessary for the telescope's motion. The kinematic energy of the system is described in (2), while the potential energy is described in (3).

$$ K = \frac{1}{2}I_{z_1}^2\dot{q_1} + \frac{1}{2}m_2\left[L_2^2\dot{q_2}^2 + L_2^2cos(q_2)^2\dot{q_1}^2\right] + \frac{1}{2}I_{y_2}\dot{q_2}^2 + \frac{1}{2}I_{z_2}\dot{q_1}^2 \tag{2} $$

$$ U = -m_1\frac{L_1}{2}g - m_2g\left(L_1 + sin(q_2)Cg_2\right) \tag{3} $$

Here, I_{z_1} is the inertia of link 1 over its Z axis, m_1 is the mass of link 1, I_{y_2} and I_{z_2} are the inertias of link 2 over its Y axis and Z axis, respectively. Finally, m_2 is the mass of link 2, g is the Earth's gravity, and Cg_2 is the center of gravity of link 2. The applied torques corresponding to each link are calculated using the Lagrangian (L in (4)), and these torques (τ_i in (4)) are obtained from the partial derivatives of the Lagrangian for each i-th link.

$$ L = K - U \qquad \tau_i = \frac{d}{dt}\frac{\partial L}{\partial \dot{q}_i} - \frac{\partial L}{\partial q_i} \tag{4} $$

Finally, the dynamic equation is described by (5).

$$ M(q)\ddot{q} + C(q,\ddot{q}) + \Gamma(q) = \tau \tag{5} $$

Where $q = [q_1, q_2]^T$ and $\tau = [\tau_1, \tau_2]^T$ are the telescope angles and applied torques on the telescope joints, respectively.$M(q)$ is the inertia matrix defined in (6), $C(q,\ddot{q})$ is the Coriolis matrix defined in (7), and $\Gamma(q)$ is the gravity matrix torque defined in (8), assuming that the center of gravity of link 2 (Cg_2) is not located over the telescope joint.

$$ M(q) = \begin{bmatrix} I_{z_1}^2 + m_2L_2^2cos(q_2)^2 + I_{z_2} & 0 \\ 0 & m_2L_2^2 + I_{y_2} \end{bmatrix} \tag{6} $$

$$ C(q,\ddot{q}) = \begin{bmatrix} 0 \\ -m_2L_2^2cos(q_2)sin(q_2)\dot{q_1}^2 \end{bmatrix} \tag{7} $$

$$ \Gamma(q) = \begin{bmatrix} 0 \\ m_2gcos(q_2)Cg_2 \end{bmatrix} \quad \text{Where: } Cg_2 = \frac{L_2}{2} \tag{8} $$

III. Control Design

Choosing $x_1 = q$ and $\dot{x_1} = x_2$, the system (5) can be represented in the canonical form (9).

$$ \begin{cases} \dot{x_1} = x_2 \\ \dot{x_2} = F_a(x) + G_a(x)u \\ Y = x_1 \end{cases} \tag{9} $$

Where:

$$ F_a(x) = -M(x)^{-1}\left[C(x,\dot{x}) + \Gamma(x)\right] $$

$$ G_a(x) = M(x)^{-1} $$

In (9), $Y \in \Re_{2x1}$, the function $F_a(x) \in \Re_{2x1}$ is nonlinear, and $G_a(x) \in \Re_{2x2}$ is a diagonal positive definite matrix. Since these functions are usually unknown, a robust controller proposed by [8] is used to control each link individually, as depicted in Fig. 3.

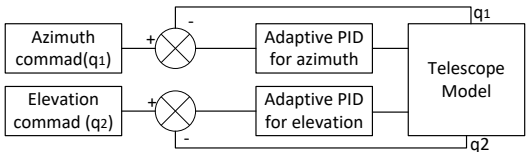

Fig. 3: Control algorithm proposed for the telescope mount.

A. Control Algorithm

In this subsection, the i-th output of the system (9) is denoted as y, the desired i-th command value is y_d, $G(x)$ is the i-th diagonal element of $G_a(x)$, and $F(x)$ is the i-th element of $F_a(x)$. In [8], the tracking error is defined as $e = y_d(t) - y(r)$, and the sliding surface is defined as (10).

$$s(t) = \dot{e}(t) + \lambda e(t) \tag{10}$$

Where λ is positive; it is proven in [8], [9] that $s(t) \to 0$ implies $e(t) \to 0$. Additionally, $\dot{s}(t)$ is calculated as shown in (11).

$$\dot{s} = \ddot{y}_d + \lambda\dot{e} - F(x) - G(x)u \tag{11}$$

According to [8], assuming that $F(x)$ and $G(x)$ are perfectly known, the ideal control u^* is defined in (12).

$$u^* = \frac{1}{G(x)}\left[-F(x) + \ddot{y}_d + \lambda\dot{e} + \alpha s + \beta tanh(s/\epsilon)\right] \tag{12}$$

Where $\alpha > 0$, $\beta > 0$ and $0 < \epsilon < 1$. By replacing (12) in (11), (13) is obtained.

$$\dot{s} = -\alpha s - \beta tanh(s/\epsilon) \tag{13}$$

To demonstrate its stability, [8] uses the Lyapunov candidate function defined in (14).

$$V = (1/2)s^2 \tag{14}$$

The Lyapunov derivative of (14) using (12) is defined in (15).

$$\dot{V} \leq -\alpha s^2 \tag{15}$$

This implies the convergence of the surface $s(t)$ towards zero. However, since the functions $F(x)$ and $G(x)$ are usually unknown; [8] proposes a PID adaptive controller approach to approximate the ideal control (12). The PID controller is defined in (16).

$$u = \Phi^T\theta \tag{16}$$

Where:

$$\Phi = \left[e(t), \int_0^t e(t), \dot{e}(t)\right]^T \quad \text{and} \quad \theta = [K_p, K_i, K_d]^T \tag{17}$$

The aim is to tune θ online to minimize the squared error between the unknown ideal control (12) and the proposed PID law (16). Using (12), equation (11) can be rewritten as (18).

$$\dot{s} = \ddot{y}_d + \lambda\dot{e} - F(x) - G(x)u + \alpha s - \alpha s + \beta tanh(s/\epsilon) - \beta tanh(s/\epsilon)$$

$$\dot{s} = G(x)u^* - G(x)u - \alpha s - \beta tanh(s/\epsilon)$$

$$\dot{s} = -\alpha s - \beta tanh(s/\epsilon) + G(x)(u^* - u) \tag{18}$$

Assuming arbitrarily that the ideal control can be reached by the PID controller, (16) can be rewritten as (19), where θ^* are the parameters that make $u = u^*$.

$$u^* = \Phi^T\theta^* \tag{19}$$

The error between ideal controller u^* and u is defined as (20).

$$e_u = u^* - u = \Phi^T(e)\tilde{\theta} \tag{20}$$

Where $\tilde{\theta} = \theta^* - \theta$. Applying (20), (18) is rewritten as (21).

$$\dot{s} = -\alpha s - \beta tanh(s/\epsilon) + G(x)e_u \tag{21}$$

However, to define the cost function, e_u cannot be used because it is not measurable due to the unknown value of $G(x)$. Hence, a measurable parameter (22) is derived.

$$G(x)e_u = \dot{s} + \alpha s + \beta tanh(s/\epsilon) \tag{22}$$

To derive the adaptation law, [8] defines the cost function as (23).

$$J(\theta) = \frac{1}{2}e_u^2 = \frac{1}{2}\left(u^* - \Phi^T(e)\theta\right)^2 \tag{23}$$

A gradient-type method is then used to minimize (23).

$$\dot{\theta} = -\eta G(x)\nabla J(\theta) = \eta\Phi(e)G(x)e_u \tag{24}$$

Where $\eta > 0$, by replacing (22) in (24), the estimation law is defined as (25).

$$\dot{\theta} = \eta\Phi(e)\left(\dot{s} + \alpha s + \beta tanh(s/\epsilon)\right) \tag{25}$$

The stability of the tracking error and the closed loop is analyzed by [8] using the Lyapunov candidate function defined in (26).

$$V = \frac{1}{2}s^2 + \frac{1}{2\eta}\tilde{\theta}^T\tilde{\theta} \tag{26}$$

The derivative of (26) is calculated as (27), assuming $\dot{\theta}^* \approx 0$ due to its convergence.

$$\dot{V} = s\dot{s} - \frac{1}{\eta}\tilde{\theta}\dot{\theta} \tag{27}$$

Then, (28) is obtained by replacing (21), (25), and (22) in (27).

$$\dot{V} = -\alpha s^2 - s\beta tanh(s/\epsilon) + sG(x)e_u - G(x)e_u^2 \tag{28}$$

The inequality (29) is derived from $s^2 + 2e_u s + e_u^2 = (s + e_u)^2$.

$$|-e_u s|G(x) \leq G(x)\frac{1}{2}\left(s^2 + e_u^2\right)$$

$$-G(x)\frac{1}{2}\left(s^2 + e_u^2\right) < G(x)e_u s \leq G(x)\frac{1}{2}\left(s^2 + e_u^2\right) \tag{29}$$

Using (29) and knowing that $tanh(s/\epsilon) \geq 0$, a valid expression for $\dot{V}$ derived from (28) is obtained in (30) [8].

$$\dot{V} \leq -\alpha s^2 - G(x)e_u^2 + G(x)e_u s$$

$$\dot{V} \leq -\left(\alpha - \frac{G(x)}{2}\right) s^2 - \frac{1}{2} G(x) e_u^2 \tag{30}$$

Supposing that $\alpha \geq \bar{G}(X)/2$, where $\bar{G}(X)$ is the highest expected value of $G(x)$, $\dot{V}$ becomes a negative definite function. Therefore, the convergence of $e \to 0$ as $t \to 0$ is guaranteed.

B. Control algorithm parameters selection

The selection of adaptive control parameters, such as the learning rate, is a complex and time-consuming process. A high learning rate can improve accuracy but may cause high-frequency chattering in actuators, while a low learning rate results in smoother actuator responses but higher errors between the reference and actual output. Thus, a trade-off between robustness and control smoothness is required [10]. To optimize this process, a genetic algorithm (GA) is used to minimize the output described by a cost function (J) [11], [12]. Monte Carlo simulations with the genetic algorithm help select parameters that minimize J. The cost function flow diagram is shown in Fig. 4.

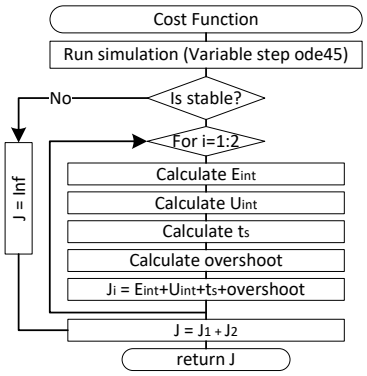

Fig. 4: Cost Function Flow diagram used for each telescope link.

Where t_s is the settlement time at $\pm 2\%$ of the steady-state value; E_{int} and U_{int} are defined in (31).

$$E_{int} = \int_0^T e^2 dt \quad ; \quad U_{int} = \int_0^T u^2 dt \tag{31}$$

IV. Results

Numerical simulations were conducted to test the proposed control algorithm, with parameters detailed in Table II.

TABLE II: Telescope physical properties

Name	Value	Units	Name	Value	Units
m_1	7	kg	I_{z_1}	0.1400	Kgm^2
m_2	10	kg	I_{y_2}	2.1895	Kgm^2
L_1	0.2	m	I_{z_2}	0.1125	Kgm^2
L_2	0.8	m	g	9.81	m/s^2

The GA library *gaoptimset* in *MATLAB* was used to tune the control algorithm, with a population size of 20 and 10 generations. The optimized vector (K) is defined in (32), and the resulting optimal parameters are shown in Table III.

$$K_i = [\lambda, \eta, \alpha, \beta, \epsilon] \quad \text{for: } i = 1, 2 \quad \text{and} \quad K = [K_1, K_2] \tag{32}$$

TABLE III: Optimized control algorithms parameters

Parameter	Azimuth control	Elevation Control
λ	0.7738	9.3296
η	8.2246	38.0034
α	2.8389	1.7763
β	0.0171	12.0062
ϵ	0.0578	0.4231
Initial Values: [Kp,ki,kd]	[0.1,0.1,0.1]	[0.1,0.1,0.1]

The simulation results with the parameters from Table III over 50 seconds are shown in Fig. 5 and Fig. 6. Fig. 5 displays the static performance for an azimuth angle of 60 deg and an elevation angle of 45 deg, with a t_s of 4.1545 seconds (azimuth) and 2.1875 seconds (elevation). The E_{int} values are 1.2998 rad-s (azimuth) and 0.4073 rad-s (elevation), while U_{int} values are 16.3436 N-m-s (azimuth) and 3.9891e+04 N-m-s (elevation). Fig. 6 shows the convergence of adaptive PID gains: for link 1, k_p = 2.5284, k_i = 0, and k_d = 1.0868; for link 2, k_p = 101.164, k_i = 35.6603, and k_d = 10.8378.

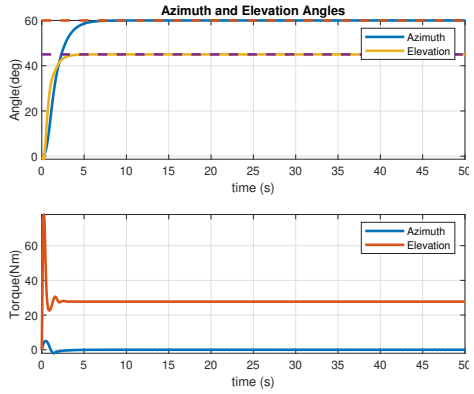

Fig. 5: Telescope Mount static performance.

In the second test, the ability to track LEO satellites was evaluated using the AJISAI satellite's orbit (see Table IV), calculated with the SPG4 propagator. Azimuth and elevation angles were computed for coordinates LLA (-16.46572, 288.50704, 2491.5050) at the Characato observatory on June 14, 2024, considering only elevation angles above 20 degrees. Results are shown in Fig. 7 and Fig. 8. Fig. 7 displays the time response with a settlement time of 5.9310 seconds for azimuth and 2.2630 seconds for elevation. U_{int} values are 495.6046 N-m-s (azimuth) and 3.0065e+05 N-m-s (elevation), while E_{int} values are 26.7643 rad-s (azimuth) and 0.5384 rad-s (elevation). Fig. 8 shows the convergence of adaptive PID gains: for link 1, k_p = 3.3510, k_i = 0, and

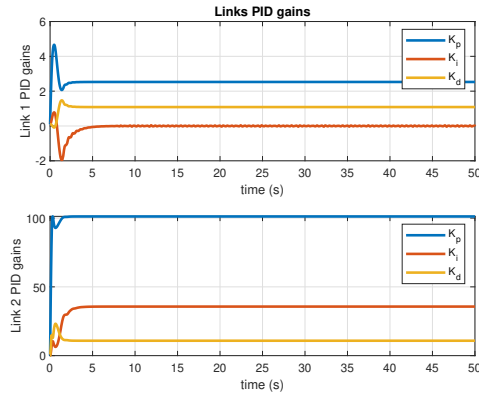

Fig. 6: Adaptive PID gains over static performance.

k_d = 1.6427; for link 2, k_p = 77.3563, k_i = 40.8737, and k_d = 27.094.

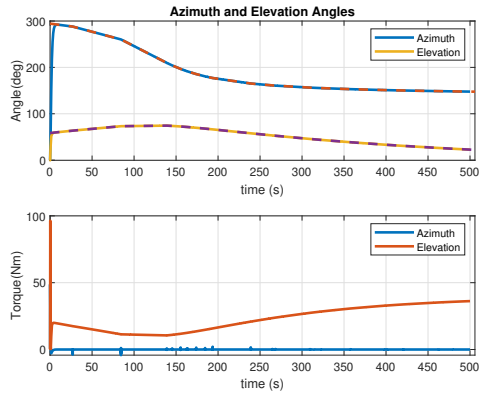

Fig. 7: Tracking performance for the Ajisai satellite.

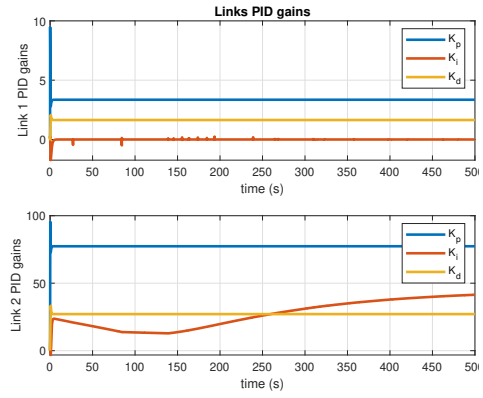

Fig. 8: Adaptive PID gains over tracking performance.

V. Conclusion

The paper presents a dynamical mathematical model of a spherical telescope for LEO satellite tracking and astronomical observations, modeled as a 2-DOF robotic arm using the Euler-Lagrange methodology. An adaptive PID controller, based on [8], is used for robust control, employing a sliding surface to determine ideal control. Adaptive PID gains are updated via the gradient method to minimize the error between ideal and actual control. A GA algorithm and random simulations were used to optimize performance. Both static and tracking evaluations showed asymptotic convergence of the telescope response without chattering in the control inputs. Simulations demonstrated PID gain convergence, with K_i in link 1 converging to zero due to gravity's nule effect on it. Finally, it was found that reducing misalignment between link 2's center of gravity and the telescope joint decreases required torque and the K_i value on Link2.

TABLE IV: Orbital Parameters of Ajisai Satellite

Parameter	Value
Orbit Type	Circular, Low Earth Orbit (LEO)
Inclination	50 degrees
Perigee	1,490 km
Apogee	1,490 km
Orbital Period	116 minutes
Eccentricity	0.001 (nearly circular)
Weight	685 kg
Diameter	2.15 meters
Number of Reflectors	1,436 retroreflectors, 318 mirrors
Launch Year	1986
Primary Purpose	Geodetic measurements

References

[1] E. Peruano. (2024) Dirección de astrofísica. [Online]. Available: https://www.gob.pe/10389-comision-nacional-de-investigacion-y-desarrollo-aeroespacial-direccion-de-astrofisica

[2] S. I. Bailey, *The Arequipa Station of the Harvard Observatory*. The Popular Science Monthly, 1904.

[3] M. Wilkinson, U. Schreiber, I. Procházka, C. Moore, J. Degnan, G. Kirchner, Z. Zhongping, P. Dunn, V. Shargorodskiy, M. Sadovnikov *et al.*, "The next generation of satellite laser ranging systems," *Journal of Geodesy*, vol. 93, no. 11, pp. 2227–2247, 2019.

[4] I. Jamshed, "Modern control laws for an articulated robotic arm," *Engineering, Technology & Applied Science Research*, vol. 9, no. 2, 2019.

[5] R. Kelly, V. Santibánes *et al.*, *Control de movimiento de robots manipuladores*. México: Pearson Educación-Prentice Hall,, 2003.

[6] A. Barrientos *et al.*, *Fundamentos de robótica*. Biblioteca Hernán Malo González, 2007.

[7] A. Okubanjo, O. Oyetola, M. Osifeko, O. Olaluwoye, and P. Alao, "Modeling of 2-dof robot arm and control," *Futo J Series (FUTO-JNLS)*, vol. 3, no. 2, pp. 80–92, 2017.

[8] A. Boubakir, S. Labiod, and T. Guerra, "Commande pid adaptative des systèmes non linéaires affines en la commande."

[9] J.-J. E. Slotine, "Applied nonlinear control," *PRENTICE-HALL google schola*, vol. 2, pp. 1123–1131, 1991.

[10] H. Leeghim, Y. Choi, and H. Bang, "Adaptive attitude control of spacecraft using neural networks," *Acta Astronautica*, vol. 64, no. 7-8, pp. 778–786, 2009.

[11] A. Lambora, K. Gupta, and K. Chopra, "Genetic algorithm-a literature review," in *2019 international conference on machine learning, big data, cloud and parallel computing (COMITCon)*. IEEE, 2019, pp. 380–384.

[12] A. K. Dey, A. Saha, and S. Ghosh, "A method of genetic algorithm (ga) for fir filter construction: design and development with newer approaches in neural network platform," *International Journal of Advanced Computer Science and Applications*, vol. 1, no. 6, 2010.